Biochimica et Biophysica Acta 1798 (2010) 2201–2208

Contents lists available at ScienceDirect

Biochimica et Biophysica Acta

journal homepage: www.elsevier.com/locate/bbamem

Dual functions of the human antimicrobial peptide LL-37—Target membrane perturbation and host cell cargo delivery

Xuan Zhang [a,1], Kamila Oglęcka [a,2], Staffan Sandgren [b], Mattias Belting [b], Elin K. Esbjörner [c,3], Bengt Nordén [c], Astrid Gräslund [a,*]

[a] Department of Biochemistry and Biophysics, Arrhenius Laboratories, Stockholm University, SE-106 91 Stockholm, Sweden
[b] Department of Clinical Sciences, Section of Oncology, Barngatan 2:1, Lund University, SE-221 85, Lund, Sweden
[c] Department of Chemical and Biological Engineering, Physical Chemistry, Chalmers University of Technology, Kemivägen 10, SE-412 96 Gothenburg, Sweden

ARTICLE INFO

Article history:
Received 28 October 2009
Received in revised form 11 December 2009
Accepted 14 December 2009
Available online 29 December 2009

Keywords:
LL-37
Antimicrobial peptide
Calcein leakage
CD
LD
Confocal microscopy
Heparan sulphate

ABSTRACT

The mechanisms behind target vs. host cell recognition of the human antimicrobial peptide LL-37 remain ill-defined. Here, we have investigated the membrane disruption capacity of LL-37 using large unilamellar vesicles (LUVs) composed of varying mixtures of POPC, POPG and cholesterol to mimic target and host membranes respectively. We show that LL-37 is unable to induce leakage of entrapped calcein from zwitterionic POPC LUVs, whereas leakage from LUVs partially composed of POPG is fast and efficient. In accordance with typical antimicrobial peptide behavior, cholesterol diminished LL-37 induced leakage. By using linear dichroism and flow oriented LUVs, we found that LL-37 orients with the axis of its induced α-helix parallel to the membrane surface in POPC:POPG (7:3) LUVs. In the same system, we also observed a time-dependent increase of the parallel α-helix LD signal on timescales corresponding to the leakage kinetics. The increased LD may be connected to a peptide translocation step, giving rise to mass balance across the membrane. This could end the leakage process before it is complete, similar to what we have observed. Confocal microscopy studies of eukaryotic cells show that LL-37 is able to mediate the cell delivery of non-covalently linked fluorescent oligonucleotides, in agreement with earlier studies on delivery of plasmid DNA (Sandgren et al., J. Biol. Chem. 279 (2004) 17951). These observations highlight the potential dual functions of LL-37 as an antimicrobial agent against bacterial target cells and a cell-penetrating peptide that can deliver nucleic acids into the host cells.

1. Introduction

The rapid development of bacterial resistance to conventional antibiotics is becoming an increasingly difficult problem that necessitates the development of new strategies to combat microbial infection. Naturally derived antimicrobial peptides (AMPs) commonly display potent broad spectrum bactericidal activities in combination with a reasonably high selectivity, rendering these macromolecules interesting as model compounds for the development of the next generation antibiotics. In contrast to conventional antibiotics which exert toxic activity by binding to specific targets, AMPs have classically been considered to act by more non-specific membrane-destabilizing mechanisms. The basis of their selectivity is thought to rely on preferential binding to the negatively charged outer leaflet of bacterial plasma membranes of microbes as compared to the predominantly zwitterionic outer leaflet of the eukaryotic plasma membrane [1]. Hallmarks for AMPs are a net positive charge and ability to adopt amphipathic secondary structures upon interaction with lipid bilayers. The latter has been suggested as crucial for the peptide-induced permeabilization of the target membrane [1,2].

LL-37 is, to this date, the only AMP identified in the human cathelicidin family. It is a 37 residue peptide ($LLGDF_5$ $FRKSK_{10}$ $EKIGK_{15}$ $EFKRI_{20}$ $VQRIK_{25}$ $DFLRN_{30}$ $LVPRT_{35}$ ES) that carries 16 charged residues in total. At neutral pH, its net charge is +6 [3]. LL-37 is a proteolytic cleavage product corresponding to the C-terminus of its precursor protein hCAP18 (human cationic antibacterial protein of

Abbreviations: AMP, antimicrobial peptide; ATR-FTIR, Attenuated Total Reflection Fourier Transform Infrared; CD, circular dichroism; CPP, cell-penetrating peptide; DPC, Dipalmitoyl Phosphatidyl Choline; DPH, 1,6-diphenyl-1,3,5-hexatriene; HS, Heparan Sulphate; LD, linear dichroism; LL-37, the human, multifunctional cathelicidin peptide, composed of 37 residues with the sequence ($LLGDF_5$ $FRKSK_{10}$ $EKIGK_{15}$ $EFKRI_{20}$ $VQRIK_{25}$ $DFLRN_{30}$ $LVPRT_{35}$ ES); LUVs, large unilamellar vesicles; MIC, minimum inhibitory concentration; MRE, mean residue ellipticity; POPC, 1-Palmitoyl-2-oleoyl-*sn*-glycero-3-phosphatidylcholine; POPG, 1-Palmitoyl-2-oleoyl-*sn*-glycero-phosphoglycerol; SDS, sodium dodecyl sulphate; SM, sphingomyelin; P/L, peptide-to-lipid

* Corresponding author. Tel.: +46 8 162450; fax: +46 8 155597.
E-mail address: astrid@dbb.su.se (A. Gräslund).

[1] On leave from Department of Pharmaceutics, School of pharmaceutical science, Peking University, Beijing, China.

[2] Present address: Institute of Bioengineering and Nanotechnology, 31 Biopolis Way, The Nanos #07-01, 138669, Singapore.

[3] Present address: Department of Chemistry, University of Cambridge, Lensfield Road, Cambridge CB2 1EW, UK.

0005-2736/$ – see front matter © 2010 Elsevier B.V. All rights reserved.
doi:10.1016/j.bbamem.2009.12.011

18 kDa) [4–6], and has been shown to be secreted by a large number of cell types throughout the human body — consequently being present in several tissues and body fluids [7]. Thus, LL-37 has potentially important roles that go beyond its antibiotic activity and hCAP18/LL-37 expression has been found to be either up- or down-regulated in various conditions of disease, implying that LL-37 is also a part of the human innate immune response [8,9].

LL-37 displays antimicrobial activity against both Gram-positive and Gram-negative bacteria at a minimum inhibitory concentration (MIC) in the <10 μg/ml range [10]. Electron micrographs of stained *E. coli* show that LL-37 causes morphological changes to the cell membranes below MIC and full lysis when MIC is reached [3]. In addition, freeze-fracture electron microscopy studies of *Candida albicans* cells subjected to MIC concentrations of LL-37 show disintegration of the cells into discrete vesicles with a concomitant efflux of cell material [11]. Therefore, it is likely that peptide-induced membrane disruption is directly involved in the antimicrobial action of LL-37.

LL-37 has been well characterized with respect to antimicrobial activity, in vivo expression and immunomodulatory function (see Dürr et al. [7] for an extensive review). Its biophysical properties, particularly in model membrane systems designed to mimic prokaryotic and eukaryotic membranes, have also been examined. It has been found that LL-37 is most effective in killing bacteria under conditions where the propensity for α-helix formation is high, and that helix formation is facilitated by the ability of certain ions to "salt out" nonpolar groups in LL-37 [12].

Regarding membrane binding, the reports about the ability of LL-37 to discriminate between zwitterionic and negatively charged lipids are still somewhat ambiguous. LL-37 can interact with both zwitterionic and net negatively charged lipid vesicles, adopting predominantly α-helical structures [3,13]. The structure of LL-37 in complex with membrane-mimetic SDS and DPC micelles has been assessed [14,15]. However, at least two groups report that there is no interaction between LL-37 and zwitterionic lipid monolayers [16,17]. There are also some indications that LL-37 membrane interactions are not entirely governed by electrostatics. Other membrane characteristics, such as acyl chain packing and membrane rigidity (introduction of sterols) and dynamics have been suggested to have a decisive role on membrane–peptide interactions. Polarized ATR-FTIR spectroscopy [3] as well as solid-state NMR [18] suggests that LL-37 is mainly oriented parallel to the lipid surface.

It has been reported that LL-37 causes membrane leakage of small ions (dissipation of potassium gradients over lipid vesicle membranes) in both zwitterionic and negatively charged large unilamellar vesicles, indicating that LL-37 is not able to selectively disrupt bacterial membranes [13,17,19]. On the other hand, the results of Björstad et al. [20] indicate at least some discrimination in the level of calcein leakage between phospholipid vesicles with compositions mimicking prokaryotic and eukaryotic cell membranes. It has been suggested that LL-37 causes membrane disruption and subsequent leakage via a detergent-like carpeting mechanism [3,18].

In the present study we systematically explore the leakage-inducing activity of LL-37 in unilamellar phospholipid vesicles (LUVs) with varied contents of zwitterionic (POPC) and negatively charged (POPG) phospholipids, in the absence and presence of cholesterol. LUVs are considered to be good and rather stable mimetic systems for cell membranes, particularly for bacteria, because of their size (typically 100 nm in diameter) which is not too far from that of a bacterial cell. LUVs have a moderate curvature and relatively large inner volume compared to small unilamellar vesicles (SUVs) which have a diameter of usually less than 50 nm. In LUVs, peptides are expected to be less affected by the tension in the membrane imposed by curvature, but for spectroscopic measurements SUVs are sometimes preferred because they cause less light scattering. Giant unilamellar vesicles (GUVs) with a diameter of about 10 μM have a size on the scale of eukaryotic cells, but they give rise to light scattering. Here we have chosen to use LUVs as membrane mimetics, which combine relatively good stability with manageable light scattering problems [21,22]. Our results provide evidence of a so-called graded mechanism of vesicle leakage in the partly negatively charged vesicles. The vesicle binding geometry is studied by means of polarized light absorption spectroscopy (linear dichroism) on α-helical LL-37 associated with shear-aligned LUVs. In view of the ongoing discussion about the sometimes converging roles of AMPs and CPPs (cell-penetrating peptides) [23], we also studied the CPP properties of LL-37, and show that LL-37 mediates the translocation of a non-covalently complexed oligonucleotide into live eukaryotic cells.

2. Materials and methods

2.1. Materials

LL-37 was synthesized by Innovagen AB (Lund, Sweden). Peptide sequence and purity (>98%) were confirmed by reverse phase HPLC and mass spectrometry. The peptide concentration was determined by quantitative amino acid analysis (hydrolysis by acid treatment followed by quantification of the amino acid content by liquid chromatography). 1-Palmitoyl-2-oleoyl-*sn*-glycero-3-phosphatidylcholine (POPC), 1-Palmitoyl-2-oleoyl-*sn*-glycero-phosphoglycerol (POPG), and cholesterol were purchased from Avanti Polar Lipids (Alabaster, US). *1,6*-diphenyl-*1,3,5*-hexatriene (DPH) was obtained from Sigma-Aldrich (Sweden). Calcein was from Fluka Biochemica (Buchs, Schweiz). Heparan sulphate (HS) (estimated M_W ~15 kDa; each HS molecule carries about 65 negative charges) was prepared as described previously [24]. The YOYO-1 label was acquired from Molecular Probes and the DNA-ON from Sigma.

2.2. Preparation of large unilamellar vesicles (LUVs)

LUVs were prepared by dissolving phospholipids and cholesterol in chloroform at desired molar ratios to ensure complete mixing of the components. The solvent was removed under a stream of nitrogen and the dried lipid film was thereafter dispersed in buffer (50 mM phosphate buffer, pH 7.4 unless stated otherwise). To obtain monodisperse, unilamellar vesicles, the dispersion was freeze-thawn six times and then extruded through two polycarbonate filters (100 nm pore size) 21 times using a manual extruder from Avanti (Alabaster, US).

2.3. Fluorescence spectroscopy

Fluorescence was measured on a Perkin Elmer LS 50B Luminescence Spectrometer interfaced with the FL WinLab software. For the calcein leakage experiments (*vide infra*) the excitation monochromator was set to 490 nm and the emission was scanned from 500 to 540 nm, with a bandwidth of 3 nm for both excitation and emission. Five consecutive scans, recorded at a scan speed of 250 nm/min, were accumulated and averaged for each data point. The temperature was set to 20 °C and a 4×10 mm quartz cuvette was used.

For the DPH fluorescence polarization experiments the excitation monochromator was set to 355 nm and the emission was recorded at 530 nm. Fluorescence measurements were conducted at 37 °C using the same cuvette and spectra collection method as described for the calcein leakage measurements. A polarization attachment (Shimadzu) was adapted to the spectrometer allowing the steady-state polarization to be determined using the following equation:

$$P = \frac{I_{VV} - GI_{VH}}{I_{VV} + GI_{VH}}; G = \frac{I_{HV}}{I_{HH}} \quad (1)$$

where I_{VV} is the emission intensity recorded with vertically polarized excitation and emission and I_{VH} is the emission intensity recorded with vertically polarized excitation and horizontally polarized

emission. The instrumental correction factor G was determined by measuring the polarized components of fluorescence of the probe with horizontally polarized excitation.

2.4. Calcein leakage from LUVs induced by LL-37

LUVs with entrapped calcein were essentially prepared as described above. The lipid film was however hydrated in 50 mM phosphate buffer, pH 7.4, containing 70 mM calcein (well above self-quenching concentration). Non-entrapped calcein was separated from the LUVs by gel filtration on two consecutive Sephadex-G25 columns (Amersham Biosciences).

Two sets of leakage experiments were performed. First, the degree of leakage was estimated as a function of peptide-to-lipid molar ratio by titrating a LUV suspension of desired composition (total lipid concentration was 100 μM) with small aliquots of peptide (from a 0.5 mM stock solution). Second, the time course of leakage was monitored at a fixed peptide-to-lipid (P/L) ratio (1:100) by measuring the fluorescence intensity as a function of time.

The degree of calcein leakage was estimated by measuring the fluorescence intensity from the released (unquenched) calcein as described above. The maximum leakage level (100%) was established by lysing the vesicles with 10% (v/v) Triton X-100 and the percent leakage value was thereafter calculated according to:

$$\%leakage = 100 \times \left[\frac{F - F_0}{F_{max} - F_0}\right] \quad (2)$$

where F_0 represents the background fluorescence intensity of the intact vesicles recorded prior to addition of peptide, F the measured fluorescence intensity after peptide addition, and F_{max} the fluorescence intensity of the lysed vesicle sample.

2.5. Calcein leakage induced by LL-37–Heparan sulphate complexes

LL-37 was mixed with heparan sulphate (HS) in molar ratios of 1:0, 1:1, 1:2, 1:4, 1:10 and 1:20. These solutions were added to 100 μM POPC:POPG (7:3) LUVs which resulted in a final concentration of 4 μM LL-37 in all experiments. The release of calcein from the LUVs was monitored at 37 °C.

2.6. DPH fluorescence polarization

To monitor the bilayer perturbation caused by LL-37 interactions, LUVs (at 200 μM lipid concentration) were doped with the membrane-bound probe DPH (2 μM). The added DPH (from a 1 mM ethanolic stock solution) was allowed to equilibrate in the membranes for 15 min before measurement. LL-37 (P/L = 0.1) was then added to the DPH-doped LUVs and left to equilibrate for an additional 10 min. The polarization was calculated according to Eq. (1).

2.7. Circular dichroism (CD) spectroscopy

CD spectra were obtained with a Jasco J-720 Spectropolarimeter equipped with a PTC-343 temperature controller. A quartz cell with an optical path length of either 0.5 mm or 1.0 mm was used. The spectral range was 190–250 nm with a resolution of 0.2 nm and a bandwidth of 1.0 nm. A scan speed of 100 nm/min with 4 s response time was employed. Spectra were collected and averaged over twenty scans at a temperature of 20 °C unless stated otherwise. All spectra were corrected for background contributions by subtraction of appropriate blanks. To assess the secondary structure of LL-37 in the presence of LUVs of different composition, 40 μM LL-37 was added to a sample of LUVs (1 mM total phospholipid concentration). The impact of temperature (0–60 °C) on the secondary structure of LL-37 (100 μM) in the absence of LUVs, was assessed in pure water.

The population of the PPII helix (also called polyproline II or left-handed 3_1 helix) was calculated from the CD amplitude of the local maximum around 220 nm (the exact wavelength of this maximum is dependent on the sequence). The population of the left-handed PPII helix was estimated from the mean residual ellipticities (MRE) at λ_{max} using the relation published by Kelly et al. [25].

$$PPII\% = \frac{[\theta]_{max} + 6100}{13,700} \times 100\% \quad (3)$$

2.8. Flow linear dichroism (LD) spectroscopy

LD was used to probe the orientation of the α-helical part of LL-37 when associated to POPC:POPG (7:3) LUVs. LD is defined as the difference in absorption of linearly polarized light oriented parallel and perpendicular to the orientation axis of a sample, according to:

$$LD = A_{II} - A_{\perp}. \quad (4)$$

Macroscopic orientation can be obtained by subjecting LUVs to shear flow in a rotating Couette cell [26,27]. The shear forces render the LUVs slightly ellipsoidal in shape and they will align with their long axes parallel to the flow direction. A peptide that binds to the membrane in an ordered fashion will exhibit LD because its absorbing transition moments display a preferential orientation. Transition moments that are oriented preferentially parallel to the lipid vesicle surface display positive LD and transition moments that are preferentially oriented parallel to the membrane normal display negative LD. LL-37 contains no aromatic residues and the only absorbing moieties are the amide chromophores of the peptide backbone. In an α-helical peptide the amide bond $\pi \rightarrow \pi^*$ transitions interact by exciton coupling, which give rise to two resultant transitions; one polarized parallel to the helix axis (observed at 208–210 nm) and one polarized perpendicular to the helix axis (observed at 190–195 nm). In addition, a weakly absorbing (forbidden) $n \rightarrow \pi^*$ transition may perhaps be observed at 220–225 nm.

LD spectra were recorded on a Jasco J-720 Spectropolarimeter equipped with an Oxley prism to obtain linearly polarized light [28]. The samples were oriented in a Couette cell with a total path length of 1 mm using a stationary shear flow of 3100 s^{-1}. Spectra were recorded between 190 nm and 350 nm at room temperature. The scan speed was 50 nm/min, the response time was 1 s, and the bandpass was 2 nm. 3 consecutive scans were collected and averaged by the computer and all spectra were corrected for background contributions by subtraction of the LD spectra recorded on the corresponding non-oriented sample (*i.e.* without rotation of the Couette cell).

LD spectra were recorded only in POPC:POPG (7:3) LUVs at a peptide-to-lipid molar ratio of approximately 0.02 and a total lipid concentration of 2.2 mM. Samples were prepared in a 5 mM phosphate buffer, pH 7.4 for maximum transparency in the far UV, and supplemented with 50% (w/w) sucrose to reduce light scattering and to increase the viscous drag and hence the degree of sample orientation [26].

2.9. Confocal microscopy

Cells were seeded at low density in 4-well chamber slides and allowed to adhere over night, and were then incubated with YOYO-1-labeled DNA oligonucleotide and LL-37 according to the figure legend. The cells were then cleared from unspecific extracellular fluorophore by brief rinsing with 1 M NaCl in PBS, followed by extensive rinsing with PBS. Live cells were then visualized using a Nikon Eclipse E800 microscope and a Bio-Rad MRC 1024 confocal laser scanning microscopy system. Collected data was analyzed using PC-compatible Laser-Sharp software.

3. Results

3.1. Leakage of entrapped calcein from LUVs

LUVs with various lipid compositions, mimicking fundamental features of prokaryotic and eukaryotic membranes were prepared with entrapped calcein. Fig. 1 shows the level of induced calcein leakage obtained by titrating incremental amounts of LL-37 to a suspension of LUVs. Each data point was recorded after 5 min incubation at 20 °C. The figure shows that neutral POPC LUVs remain intact even up to a P/L molar ratio of 0.05 which is extremely high from a physiological perspective. In contrast, considerable calcein leakage was induced in the two examined types of net negatively charged POPC:POPG LUVs. Increasing the amount of POPG in these LUVs from 30 to 70% increased the leakage efficiency to some extent, which may be explained by increased electrostatic interactions. Nearly 100% leakage is obtained for POPC:POPG (3:7) LUVs, indicating massive disruption of the lipid bilayer in this particular case. These results suggest that LL-37 behaves as a classic AMP, completely discriminating between neutral (host-like) and negatively charged (target-like) membranes. This is in contrast to what was previously reported by Oren et al. [3] who reported leakage of small monovalent cations (potassium) in both types of membranes. A potential explanation to this discrepancy is that calcein is a considerably larger molecule than potassium and thus may require more severe disruptions of the LUV membrane in order to escape.

Fig. 2 shows the time course of leakage monitored at a constant P/L of 0.01. The calcein leakage curves are biphasic, with faster kinetics for LUVs with higher negative charge. This two-phase leakage kinetics behavior with an apparent plateau, has been observed for many peptides that induce membrane leakage [29,30]. The observation of a leakage plateau can be described as due to a relaxation process by which the membrane rearranges after the peptide is added, a so-called graded leakage mechanism [23,31]. It should be noted that the flow linear dichroism signal of the peptide presented in Fig. 5 increases on a similar timescale (minutes-hours) as the relaxation observed in the leakage (*vide infra*), suggesting that we indeed can observe the slow process by which the bound peptide and/or the surrounding lipids, approach an equilibrium state. Calcein leakage is counteracted by the presence of cholesterol in the phospholipid bilayer, as observed by the addition of 20% cholesterol (on expense of POPC) to the LUVs containing 30% negative charge (Fig. 2). This is in agreement with the results by Sood et al. [13,19] and furthers the evidence for LL-37's classical AMP behavior.

Calcein leakage induced by LL-37 in partly charged LUVs is not significantly affected by incubation temperature (4, 20 and 37 °C, data not shown). We next investigated to what extent binding to heparan sulphate (HS), *i.e.* a highly polyanionic polysaccharide covering the surface of eukaryotic cells while absent on prokaryotes, could diminish LL-37-induced calcein leakage from POPC:POPG (7:3) LUVs. LL-37 was pre-incubated with fractions of HS at up to 10 times the stoichiometric ratio and the mixture was thereafter added to the LUVs at 20 °C. Despite HS being strongly negatively charged and thus potentially prone to electrostatically interact with cationic LL-37, only minor effects on the induced calcein leakage were found (Supplementary information, Table S1).

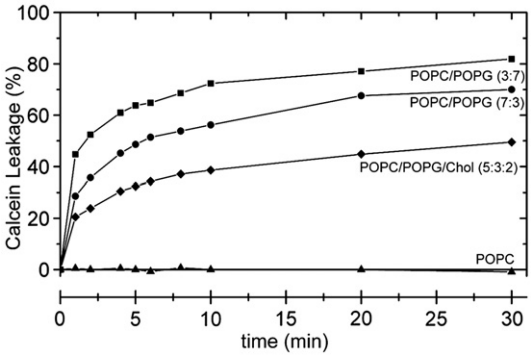

Fig. 2. LL-37 induced leakage of entrapped calcein from LUVs composed of POPC (-▲-), POPC:POPG:Cholesterol (5:3:2) (-♦-), POPC:POPG (7:3) (-●-), and POPC:POPG (3:7) (-■-) as a function of time. The peptide-to-lipid ratio was 0.01 and the total lipid concentration was 100 μM. The experiments were performed at 20 °C.

3.2. Secondary structures of LL-37

Initial CD studies showed LL-37 to be mainly in a random coil conformation at 20 °C in water, in agreement with previous observations [12]. However, the CD spectra of LL-37 in pure water revealed a temperature-dependent equilibrium between a left-handed PPII helix and a disordered random coil secondary structure, which dominates at higher temperatures (Fig. 3). The population of the left-handed PPII helix, as calculated according to Eq. (3), changed from 39% to 17% when the temperature was increased from 0 °C to 60 °C. A similar behavior has been observed previously with other peptides of similar length, e.g. the negatively charged amyloid Aβ(1–40) peptide involved in Alzheimer's disease [32]. The temperature-dependent ability to form a PPII helix provides an explanation to why the Aβ peptide is best soluble at low temperature, where the PPII helix favors hydrogen bonding interactions between peptide backbone atoms and the aqueous solvent [33]. The current data indicates that LL-37

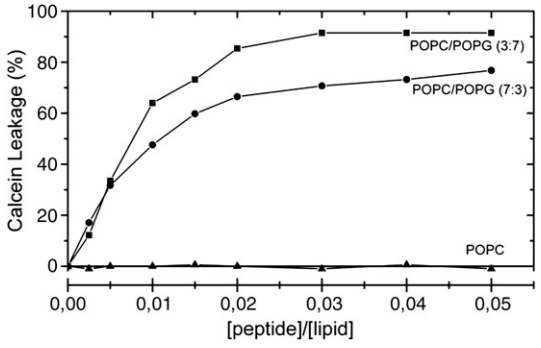

Fig. 1. LL-37 induced leakage of entrapped calcein from LUVs composed of POPC (-▲-), POPC:POPG (7:3) (-●-), or POPC:POPG (3:7) (-■-) as a function of peptide-to-lipid molar ratio, [peptide]/[lipid]. Data was collected while titrating LUVs with increasing amounts of peptide. The samples were incubated for 5 min prior to measurement and further addition of peptide. The total lipid concentration was 100 μM and the experiments were performed at 20 °C.

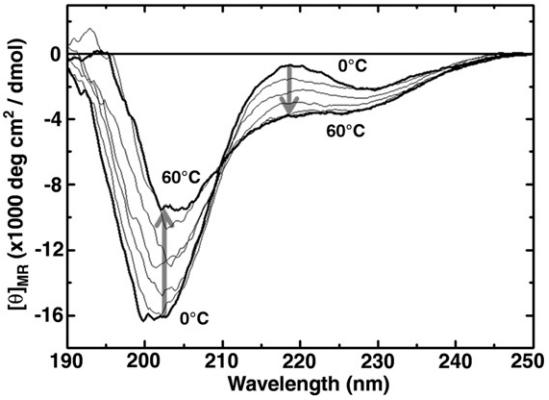

Fig. 3. CD spectra of LL-37 (100 μM) in distilled water as a function of temperature. Spectra were recorded in 10 °C intervals ranging from 0 to 60 °C (the initial and final spectra are marked in bold). The population of left-handed PPII helix decreased as the temperature and population of random coil increased.

exhibits a similar conformational plasticity, which becomes particularly interesting in the light of the suggestions that LL-37 [3,19], like the Aβ peptide [34], may exert its membrane perturbing activity via the formation of cytotoxic oligomeric assemblies.

We next attempted to mimic the effect of eukaryotic cell-surface associated HS on the secondary structure of LL-37, by adding water-soluble fractions of HS to a peptide solution. Additions of HS in amounts up to twice the weight concentration of LL-37 did not significantly change the random coil CD spectrum of the peptide, indicating lack of specific interactions inducing secondary structure (Supplementary information, Fig. S1). In experiments with fluorescently labeled HS we could however observe LL-37-induced fluorescence quenching (data not shown), suggesting that LL-37 and HS indeed form complexes, although this is only weakly manifested in secondary structure and calcein leakage induction.

The CD spectra of LL-37 in the presence of POPC and POPC:POPG (3:7) LUVs at 20 °C are shown as Fig. 4. LL-37 in the presence of POPC generates a CD spectrum clearly different from that of a random coil/PPII spectrum (Fig. 3). The spectral shape suggests a weakly forming secondary structure, possibly a distorted α-helix. In complex with the partly negatively charged LUVs (POPC:POPG (3:7)) LL-37 adopts a dominant α-helical structure, evidenced by the shape of its CD spectrum (Fig. 4). Thus, in the presence of negatively charged membranes, LL-37 behaves as a typical amphipathic peptide.

3.3. LL-37 orientation in POPC:POPG (7:3) membranes

Under conditions where LL-37 forms a partial α-helix when bound to lipid membranes, it is possible to use flow LD spectroscopy to investigate the orientation of the peptide α-helix with respect to the lipid bilayer. Fig. 5 shows LD spectra of LL-37 in shear-oriented POPC:POPG (7:3) LUVs recorded immediately upon addition of peptide to a suspension of LUVs, and after 1 h incubation. The positive LD centered at 210 nm arises from the amide $\pi \rightarrow \pi^*$ transitions of the peptide bond. In an α-helix these interact by exciton coupling and give rise to two transitions: one at a longer wavelength ~208 nm (polarized parallel to the helix axis), and one at a shorter wavelength ~195 nm (polarized perpendicular to the helix axis). The positive signature of the peak in the LD spectra shown in Fig. 5 therefore indicates that the α-helical part of LL-37 is on the average oriented parallel to the membrane surface, in agreement with previous studies using polarized ATR-FTIR and solid-state NMR [3]. The peptide bond $n \rightarrow \pi^*$ transitions are orthogonal to the $\pi \rightarrow \pi^*$ transitions and should in principle appear as a negative peak at 220–225 nm. This cannot be observed in Fig. 5, thus confirming the weak nature of these transitions compared to the $\pi \rightarrow \pi^*$. In addition, we observed a significant increase in the LD signal on a time scale of about an hour

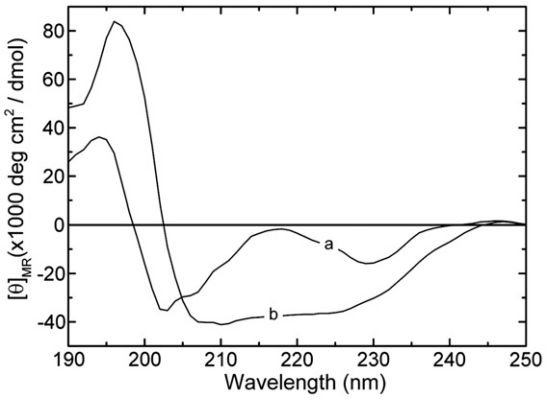

Fig. 4. CD spectra of LL-37 recorded in the presence of (a) POPC and (b) POPC:POPG (3:7) LUVs at 20 °C. The peptide concentration was 40 μM and the lipid concentration was 1 mM.

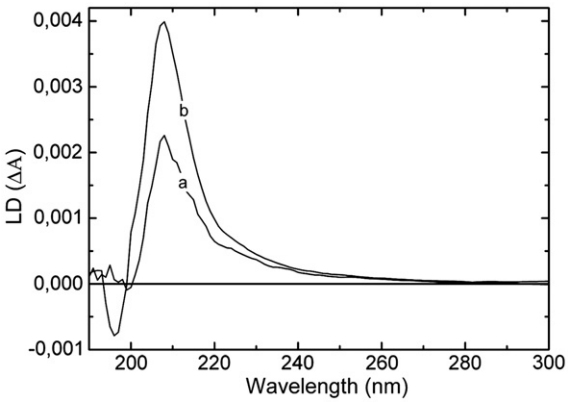

Fig. 5. Linear dichroism (LD) spectra of LL-37 bound to POPC:POPG (7:3) LUVs recorded immediately after mixing (a) and after 1 h incubation at ambient temperature (b). The peptide-to-lipid molar ratio was approximately 0.02. The positive LD peak at 208 nm shows that the α-helical part of LL-37 is oriented in parallel to the membrane surface.

(Fig. 5), which indicates that the peptide, and/or the lipid vesicle membrane, obtains a higher degree of order. This rearrangement occurs on the same time scale as the calcein leakage builds up and reaches a maximum plateau, suggesting that these processes may be related.

3.4. DPH polarization

The effect of LL-37 on the membrane order/fluidity was studied using LUVs of varying membrane compositions (in terms of POPC, POPG and cholesterol), labeled with the fluorescent probe DPH (*1,6*-diphenyl-*1,3,5*-hexatriene). DPH intercalates into lipid bilayers and its excited state is sensitive to the rigidity of its surroundings. Therefore, fluorescence polarization (and anisotropy) can be used to monitor changes in membrane order upon addition of ligands to a lipid bilayer.

Table 1 shows the fluorescence polarization from DPH in LUVs of different compositions with or without LL-37 at the P/L ratio of 0.10. The experiments were repeated 4 times for each condition, and an experimental uncertainty was estimated. As expected, the differences in DPH polarization without and with peptide are relatively small. However, for the negatively charged LUVs it is apparent that there is an increase in the DPH polarization, and hence a decrease in membrane fluidity, when the peptide is added.

3.5. LL-37 mediated delivery of DNA oligonucleotide into eukaryotic cells

Fig. 6, lower panels, show confocal microscopy images of a fluorophore-labeled, 21-mer DNA oligonucleotide inside live COS-7 cells after delivery as non-covalent complexes with LL-37. The composition of the complex is about 1/1 peptide/DNA basepair, *i.e.* generating complexes where the positive charge provided by the peptide is in excess of the negative charge provided by the phosphate

Table 1
Changes in steady-state fluorescence polarization of DPH (incorporated into LUVs of different compositions) upon addition of LL-37. The lipids were either pure POPC or POPC/POPG or POPC/POPG/cholesterol at the indicated ratios. The total lipid concentration was 200 μM and the LUVs were pre-incubated with 2 μM DPH for 10 min. P/L is the peptide-to-lipid molar ratio and ΔP is the change in polarization after addition of the peptide. The temperature was 37 °C. All measurements were repeated 4 times and an average uncertainty (standard deviation) is indicated.

P/L	POPC	POPC/POPG (7/3)	POPC/POPG (3/7)	POPC/POPG/Chol (5/3/2)
0	0.185 ± 0.012	0.139 ± 0.007	0.146 ± 0.002	0.186 ± 0.001
0.1	0.165 ± 0.014	0.162 ± 0.015	0.212 ± 0.010	0.207 ± 0.007
ΔP	−0.020	+0.023	+0.056	+0.021

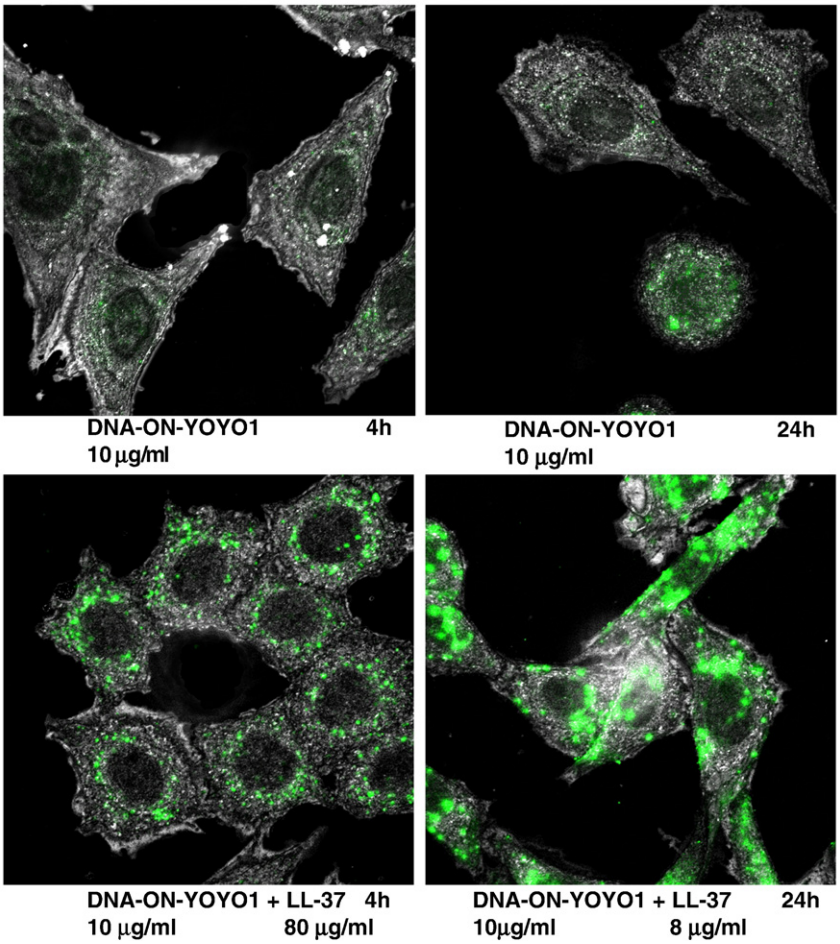

Fig. 6. Confocal microscopy images of live COS-7 cells incubated with YOYO-1-labeled DNA oligonucleotide complexed with LL-37 peptide (20 μM) for 4 h (lower left panel) and 24 h (lower right panel). Upper left and right panels show the corresponding control experiments in the absence of LL-37. In the presence of LL-37 the punctuate staining indicates vesicular uptake of the complexes. Also at the later time point (lower right panel) the DNA oligonucleotide distribution remains mainly vesicular, indicating limited vesicular escape.

groups of DNA. In the absence of LL-37 the cellular uptake is insignificant under similar conditions, as seen in the upper panels of Fig. 6. The distinct, punctuate fluorescence signal at 4 h of LL-37–DNA complex incubation (Fig. 6, lower left panel) suggests endocytosis as the major pathway of membrane translocation, and that general cytoplasmic delivery (endosomal escape) is not very efficient. The escape of endocytosed cargo molecules should occur before the endosome has developed into/fused with a lysosome if the cargo is to be delivered intact to the cytoplasm. After 24 h of incubation (Fig. 6, lower right panel), the distribution of internalized DNA appears as more diffuse, which together with nuclear localization suggests some leakage of DNA oligonucleotides from endocytic vesicles.

4. Discussion

The present results of LL-37 interaction with model membranes give an unambiguous picture of its discrimination between zwitterionic and negatively charged membranes in systematically varied and well defined lipid LUV model systems. The zwitterionic membranes are not rendered permeable for the enclosed relatively large calcein molecules, whereas the partly negatively charged membranes are affected in relative proportion to the degree of headgroup charges (Figs. 1 and 2). The leakage results extend previous observations using LUVs of other compositions [19]. For the negatively charged membranes, the addition of peptide decreases the membrane fluidity (Table 1).

The calcein leakage from partly negatively charged LUVs occurs by a so-called graded mechanism observed on a min h time scale (Fig. 2). The orientation of LL-37 in the membrane is predominantly with the axis of its induced α-helix parallel to the lipid bilayer surface, as concluded from the linear dichroism (LD) of the amide chromophores in the peptide (Fig. 5), and which is in agreement with previous studies using other methods and membrane preparations [3,18]. Interestingly, we could observe how the LD of these transitions increased on the same timescale as the peptide-induced calcein leakage reached a plateau in Fig. 2. This indicates that we can probe changes in the peptide orientation (or in the lipid environment around the peptide) leading to a "healing" or return of membrane integrity. In a more detailed model of membrane leakage, the observed increase in LD could be connected to a peptide translocation step and an establishment of a final mass balance across the membrane, which should end the calcein leakage according to the model of graded release [29].

Glycosaminoglycans in biological fluids efficiently inhibit the antibacterial effects of LL-37 [35] and cell-surface proteoglycans are necessary for LL-37-mediated uptake of plasmid DNA [24]. It was therefore a somewhat surprising result in our model system studies that HS, a major polyanionic polysaccharide specifically found on the surface of eukaryotic cells, only weakly affected the leakage-inducing activity (Table S1) and the random coil CD spectrum of LL-37 (Fig. S1). However, the fluorescence quenching experiments revealed LL-37–HS complex formation, as would be expected from the electrostatic interactions. Obviously the proteoglycan interaction, as it is modeled in the present system, is not strong enough to significantly affect neither the secondary structure nor the leakage induction activity of LL-37. These data suggest that the relative resistance of eukaryotic

cells to the cytotoxic effect of LL-37 is not only explained by their overall expression of HS, but also by their membrane architecture and composition, particularly the presence/absence of charged headgroups. In further support of this notion, in a cell viability assay HS-deficient cells did not respond differently to LL-37 peptide treatment as compared with HS-expressing wild-type cells (S. Sandgren and M. Belting, unpublished observation).

The CPP property of LL-37 is shown by its ability to mediate delivery of a non-covalent complex with a fluorescently labeled oligonucleotide into eukaryotic cells (Fig. 6). These results are in agreement with previous experiments showing LL-37 mediated delivery of plasmid DNA into mammalian cells [24]. Recent studies also show that LL-37 forms large aggregated complexes with released "self-DNA" and delivers DNA into dendritic cells, thereby triggering an autoimmune response linked to psoriasis [8]. The present results highlight the potential secondary role of LL-37 as a mediator of cell delivery of nucleic acids (or possibly other negatively charged molecules or assemblies). The confocal micrographs in Fig. 6 show that the intracellular localization of LL-37–DNA complexes is vesicular with only minor leakage of DNA oligonucleotide into the cytosol/nuclear compartment, indicating that endocytosis, possibly macropinocytosis [36], is the mechanism of cargo delivery into the cells. The LL-37-mediated cell delivery is similar to that reported for fluorescent analogues of the antimicrobial peptides magainin and buforin (of frog and toad origin, respectively), although the detailed cell translocation mechanisms may differ and also depend on variables such as cell type and presence and nature of cargo [37]. Previous studies [24] have shown that LL-37 is not cytotoxic to eukaryotic cells in concentrations up to 10 μM, whereas *E. coli* cells are killed at concentrations below 3 μM. The results presented here, where the concentration of LL-37 in Fig. 6 is 20 μM without any drastic effects on the cell images, suggest that the CPP activity of LL-37 on eukaryotic cells is valid up to quite high concentrations, compared to the concentrations required for the antimicrobial activity on bacterial cells.

In conclusion, our results are in agreement with a straightforward model of the effect of LL-37 on negatively charged bacterial target membranes: It binds to the membrane surface, whereupon α-helical structure is induced with the helix axis parallel to the membrane surface. At a relatively high peptide concentration (micromolar, with P/L 0.05) the membrane is made leaky which should model toxicity in a biological system. Under similar conditions, a zwitterionic membrane, representing a eukaryotic host cell, is not made leaky by LL-37. However, when LL-37 acts on the real membranes of eukaryotic cells together with external DNA, it is able to mediate transfer of the DNA into the cells, thereby demonstrating its activity as a CPP, possibly acting by a biological endocytotic mechanism rather than by direct membrane penetration.

Acknowledgements

This study was supported by the Swedish Research Council and by the Swedish Cancer Society.

Appendix A. Supplementary data

Supplementary data associated with this article can be found, in the online version, at doi:10.1016/j.bbamem.2009.12.011.

References

[1] M. Zasloff, Antimicrobial peptides of multicellular organisms, Nature 415 (2002) 389–395.
[2] K. Matsuzaki, Why and how are peptide–lipid interactions utilized for self-defense? Magainins and tachyplesins as archetypes, Biochim. Biophys. Acta 1462 (1999) 1–10.
[3] Z. Oren, J.C. Lerman, G.H. Gudmundsson, B. Agerberth, Y. Shai, Structure and organization of the human antimicrobial peptide LL-37 in phospholipid membranes: relevance to the molecular basis for its non-cell-selective activity, Biochem. J. 341 (Pt 3) (1999) 501–513.
[4] G.H. Gudmundsson, B. Agerberth, J. Odeberg, T. Bergman, B. Olsson, R. Salcedo, The human gene FALL39 and processing of the cathelin precursor to the antibacterial peptide LL-37 in granulocytes, Eur. J. Biochem. 238 (1996) 325–332.
[5] J.W. Larrick, M. Hirata, R.F. Balint, J. Lee, J. Zhong, S.C. Wright, Human CAP18: a novel antimicrobial lipopolysaccharide-binding protein, Infect. Immun. 63 (1995) 1291–1297.
[6] O. Sørensen, J.B. Cowland, J. Askaa, N. Borregaard, An ELISA for hCAP-18, the cathelicidin present in human neutrophils and plasma, J. Immunol. Methods 206 (1997) 53–59.
[7] U.H. Dürr, U.S. Sudheendra, A. Ramamoorthy, LL-37, the only human member of the cathelicidin family of antimicrobial peptides, Biochim. Biophys. Acta 1758 (2006) 1408–1425.
[8] R. Lande, J. Gregorio, V. Facchinetti, B. Chatterjee, Y.H. Wang, B. Homey, W. Cao, B. Su, F.O. Nestle, T. Zal, I. Mellman, J.M. Schroder, Y.J. Liu, M. Gilliet, Plasmacytoid dendritic cells sense self-DNA coupled with antimicrobial peptide, Nature 449 (2007) 564–569.
[9] I. Nagaoka, H. Tamura, M. Hirata, An antimicrobial cathelicidin peptide, human CAP18/LL-37, suppresses neutrophil apoptosis via the activation of formyl-peptide receptor-like 1 and P2X7, J. Immunol. 176 (2006) 3044–3052.
[10] J. Turner, Y. Cho, N.N. Dinh, A.J. Waring, R.I. Lehrer, Activities of LL-37, a cathelin-associated antimicrobial peptide of human neutrophils, Antimicrob. Agents Chemother. 42 (1998) 2206–2214.
[11] A.L. den Hertog, J. van Marle, H.A. van Veen, W. Van't Hof, J.G. Bolscher, E.C. Veerman, A.V. Nieuw Amerongen, Candidacidal effects of two antimicrobial peptides: histatin 5 causes small membrane defects, but LL-37 causes massive disruption of the cell membrane, Biochem. J. 388 (2005) 689–695.
[12] J. Johansson, G.H. Gudmundsson, M.E. Rottenberg, K.D. Berndt, B. Agerberth, Conformation-dependent antibacterial activity of the naturally occurring human peptide LL-37, J. Biol. Chem. 273 (1998) 3718–3724.
[13] R. Sood, P.K. Kinnunen, Cholesterol, lanosterol, and ergosterol attenuate the membrane association of LL-37(W27F) and temporin L, Biochim. Biophys. Acta 1778 (2008) 1460–1466.
[14] G. Wang, Structures of human host defense cathelicidin LL-37 and its smallest antimicrobial peptide KR-12 in lipid micelles, J. Biol. Chem. 283 (2008) 32637–32643.
[15] F. Porcelli, R. Verardi, L. Shi, K.A. Henzler-Wildman, A. Ramamoorthy, G. Veglia, NMR structure of the cathelicidin-derived human antimicrobial peptide LL-37 in dodecylphosphocholine micelles, Biochemistry 47 (2008) 5565–5572.
[16] F. Neville, M. Cahuzac, O. Konovalov, Y. Ishitsuka, K.Y. Lee, I. Kuzmenko, G.M. Kale, D. Gidalevitz, Lipid headgroup discrimination by antimicrobial peptide LL-37: insight into mechanism of action, Biophys. J. 90 (2006) 1275–1287.
[17] E. Sevcsik, G. Pabst, W. Richter, S. Danner, H. Amenitsch, K. Lohner, Interaction of LL-37 with model membrane systems of different complexity: influence of the lipid matrix, Biophys. J. 94 (2008) 4688–4699.
[18] K.A. Henzler Wildman, D.K. Lee, A. Ramamoorthy, Mechanism of lipid bilayer disruption by the human antimicrobial peptide, LL-37, Biochemistry 42 (2003) 6545–6558.
[19] R. Sood, Y. Domanov, M. Pietiainen, V.P. Kontinen, P.K. Kinnunen, Binding of LL-37 to model biomembranes: insight into target vs host cell recognition, Biochim. Biophys. Acta 1778 (2008) 983–996.
[20] A. Björstad, G. Askarieh, K.L. Brown, K. Christenson, H. Forsman, K. Onnheim, H.N. Li, S. Teneberg, O. Maier, D. Hoekstra, C. Dahlgren, D.J. Davidson, J. Bylund, The host defense peptide LL-37 selectively permeabilizes apoptotic leukocytes, Antimicrob. Agents Chemother. 53 (2009) 1027–1038.
[21] A. Gräslund, L.E.G. Eriksson, Biophysical Studies of Cell-penetrating Peptides, in: Ü. Langel (Ed.), CRC Handbook of Cell Penetrating Peptides, CRC Press, 2002, pp. 223–244.
[22] L. Mäler, A. Gräslund, Artificial Membrane Models for the Study of Macromolecular Delivery, in: M. Belting (Ed.), Methods in Molecular Biology, vol. 480, Humana Press, 2009, pp. 129–139.
[23] P.F. Almeida, A. Pokorny, Mechanisms of antimicrobial, cytolytic, and cell-penetrating peptides: from kinetics to thermodynamics, Biochemistry 48 (2009) 8083–8093.
[24] S. Sandgren, A. Wittrup, F. Cheng, M. Jonsson, E. Eklund, S. Busch, M. Belting, The human antimicrobial peptide LL-37 transfers extracellular DNA plasmid to the nuclear compartment of mammalian cells via lipid rafts and proteoglycan-dependent endocytosis, J. Biol. Chem. 279 (2004) 17951–17956.
[25] M.A. Kelly, B.W. Chellgren, A.L. Rucker, J.M. Troutman, M.G. Fried, A.F. Miller, T.P. Creamer, Host–guest study of left-handed polyproline II helix formation, Biochemistry 40 (2001) 14376–14383.
[26] M. Ardhammar, P. Lincoln, B. Nordén, Invisible liposomes: refractive index matching with sucrose enables flow dichroism assessment of peptide orientation in lipid vesicle membrane, Proc. Natl. Acad. Sci. U.S.A. 99 (2002) 15313–15317.
[27] M. Ardhammar, N. Mikati, B. Nordén, Chromophore orientation in liposome membranes probed with flow dichroism, J. Am. Chem. Soc. 120 (1998) 9957–9958.
[28] B. Nordén, M. Kubista, T. Kurucsev, Linear dichroism spectroscopy of nucleic acids, Q. Rev. Biophys. 25 (1992) 51–170.
[29] A. Arbuzova, G. Schwarz, Pore-forming action of mastoparan peptides on liposomes: a quantitative analysis, Biochim. Biophys. Acta 1420 (1999) 139–152.
[30] M.J. Choi, S.H. Kang, S. Kim, J.S. Chang, S.S. Kim, H. Cho, K.H. Lee, The interaction of an antimicrobial decapeptide with phospholipid vesicles, Peptides 25 (2004) 675–683.
[31] A. Andersson, J. Danielsson, A. Gräslund, L. Mäler, Kinetic models for peptide-induced leakage from vesicles and cells, Eur. Biophys. J. 36 (2007) 621–635.

[32] J. Danielsson, J. Jarvet, P. Damberg, A. Graslund, The Alzheimer beta-peptide shows temperature-dependent transitions between left-handed 3-helix, beta-strand and random coil secondary structures, FEBS J. 272 (2005) 3938–3949.
[33] B.W. Chellgren, T.P. Creamer, Effects of H2O and D2O on polyproline II helical structure, J. Am. Chem. Soc. 126 (2004) 14734–14735.
[34] W.L. Klein, G.A. Krafft, C.E. Finch, Targeting small Abeta oligomers: the solution to an Alzheimer's disease conundrum? Trends Neurosci. 24 (2001) 219–224.
[35] W. Baranska-Rybak, A. Sonesson, R. Nowicki, A. Schmidtchen, Glycosaminoglycans inhibit the antibacterial activity of LL-37 in biological fluids, J. Antimicrob. Chemother. 57 (2006) 260–265.
[36] M.C. Kerr, R.D. Teasdale, Defining macropinocytosis, Traffic 10 (2009) 364–371.
[37] K. Takeshima, A. Chikushi, K.K. Lee, S. Yonehara, K. Matsuzaki, Translocation of analogues of the antimicrobial peptides magainin and buforin across human cell membranes, J. Biol. Chem. 278 (2003) 1310–1315.